The Meteoritical Society

Meteoritics & Planetary Science 43, Nr 1/2, 353–365 (2008)
Abstract available online at http://meteoritics.org

Quantitative organic and light-element analysis of comet 81P/Wild 2 particles using C-, N-, and O-μ-XANES

George D. CODY[1*], Harald ADE[2], Conel M. O'D. ALEXANDER[3], Tohru ARAKI[2], Anna BUTTERWORTH[4], Holger FLECKENSTEIN[5], George FLYNN[6], Mary K. GILLES[7], Chris JACOBSEN[5], A. L. D. KILCOYNE[7, 8], Keiko MESSENGER[9], Scott A. SANDFORD[10], Tolek TYLISZCZAK[7, 8], Andrew J. WESTPHAL[4], Susan WIRICK[5], and Hikaru YABUTA[1]

[1]Geophysical Laboratory, Carnegie Institution of Washington, Washington, D.C., USA
[2]Department of Physics, North Carolina State University, Raleigh, North Carolina, USA
[3]Department of Terrestrial Magnetism, Carnegie Institution of Washington, Washington, D.C., USA
[4]Space Sciences Laboratory, University of California, Berkeley, California, USA
[5]Department of Physics, State University of New York, Stony Brook, New York, USA
[6]Department of Physics, State University of New York, Plattsburgh, New York, USA
[7]Chemical Science Devision, Lawrence Berkeley National Laboratory, Berkeley, California, USA
[8]Advanced Light Source, Lawrence Berkeley National Laboratory, Berkeley, California, USA
[9]Engineering Science Contract Group, NASA Johnson Space Center, Houston, Texas, USA
[10]Astrophysics Branch, NASA-Ames Research Center, Moffett Field, California, USA
*Corresponding author. E-mail: g.cody@gl.ciw.edu

(Received 14 May 2007; revision accepted 13 September 2007)

Abstract–Synchrotron-based soft X-ray micro-analysis was performed on particles extracted from the Stardust aerogel collector in order to obtain detailed organic functional group information on any organic solids captured as part of the Principal Examination suite of analyses for samples from comet 81P/Wild 2. It is observed that cometary organic carbon captured in aerogel is present in a number of different manifestations and often intimately associated with silicates. Carbon X-ray absorption near edge structure (XANES) spectra reveal considerable chemical complexity in all of the organic particles studied so far. Universally, the comet 81P/Wild 2 organic particles contain low concentrations of aromatic and/or olefinic carbon relative to aliphatic and heteroatom-containing functional groups, e.g., amide, carboxyl, and alcohol/ethers. N-XANES confirms the presence and assignments of these functional groups. In general, the XANES data record considerable chemical complexity across the range of organic samples currently analyzed. The atomic ratios, N/C and O/C, derived from XANES data reveal a wide range in heteroatom content; in all cases these elemental ratios are higher than that of primitive meteoritic organic matter. The wide range in chemistry, both in elemental abundances and specific organic functional groups, suggests that the comet 81P/Wild 2 organic solids may have multiple origins.

INTRODUCTION

The Stardust comet sample return mission from comet 81P/Wild 2 provides an unprecedented opportunity to assess the organic chemistry of what may be the most primitive solar system material, providing a link to the molecular cloud material that was the ultimate source of the matter from which our solar system originated. Prior to the Stardust mission, our understanding of the early history of the solar system, in terms of extraterrestrial organic carbon, has been restricted to the analysis of chondrites and interplanetary dust particles (IDPs). In the case of the former, it is clearly evident that the parent body accretion and subsequent alteration has altered the organic matter to an unknown extent from its most primitive origins (e.g., Cody and Alexander 2005; Alexander et al. 2007). In the case of IDPs, thermal processing due to atmospheric entry heating may also transform labile organic matter (Flynn et al. 2003). In the case of the Stardust mission to comet 81P/Wild 2, sample capture was designed to be as benign as possible given the constraints imposed on Discovery-class missions (Brownlee et al. 2006). Silica aerogel, with a density of 5 to 50 mg/cm^3, provides a means of

slowing down very high-velocity particles (~6 km/s relative velocity) relatively gently. Nevertheless, it appears inevitable, that some heating must have occurred during the short period of particle deceleration. A high degree of heating will lead to some chemical processing. The outstanding question is: how hot did the organics get and for how long were they heated?

From the perspective of the organic analysis/examination, the crux of the problem is to obtain the relative abundance of organic functional groups within organic particles extracted from the aerogel collectors and place these data into context with information already available on the state of extraterrestrial organic matter in pristine and thermally processed chondritic meteorites. The chemical analysis of organic matter contained within IDPs constitutes a challenge similar to that facing analysis of organic matter in Stardust particles. First, only IDPs with diameters on the order of tens of micrometers are considered small enough to have escaped extensive entry heating (Flynn et al. 2003); in the case of Stardust, most of the particles captured are in the <10 μm size range (Hörz et al. 2006). Second, organic matter in IDPs is dispersed amid mineral grains, e.g., olivine, pyroxene, and the glass with embedded metals and sulfides (GEMs) in particles that are heterogeneous at scales less than a micron (see, for example, Reitmeijer 1998 and references therein). Preliminary analyses reveal that the Stardust particles share similar fine-scale heterogeneity (Brownlee et al. 2006; Flynn et al. 2006; Zolensky et al. 2006). Obtaining a quantitative analysis of the organics contained within these particles provides a significant challenge requiring a detailed assessment of organic functional group concentrations at a spatial resolving power of less than a micron.

Over the past couple decades, the development of high-brilliance synchrotron X-ray sources coupled with advances in soft X-ray optics (soft X-rays being defined as spanning the energy range ~200 to 800 eV), have lead to the development of synchrotron-based scanning transmission X-ray microscopes (STXMs) (Jacobson et al. 1991; Kilcoyne et al. 2003). Under optimum conditions, these microscopes provide a focused monochromatic X-ray beam with a spot size on the order of 30 to 40 nm, depending on the specific zone plate used. This combination of high spatial and energy resolution yields soft X-ray spectra spanning the carbon, nitrogen, and oxygen 1s X-ray absorption edges (X-ray absorption near-edge structure [XANES] spectra) of submicron domains and provides an accurate assessment of the types of the organic functionality present. These microscopes have been shown to be very useful for solving long-standing problems involving fine-scale heterogeneity in research areas such as environmental chemistry (Myneni 2002), paleontology (Boyce et al. 2002), and organic geochemistry (Cody et al. 1996). STXM μ-XANES has also been shown to be extremely useful in unravelling the complex organic chemistry of hydrous and anhydrous IDPs (Flynn et al. 2003; Keller et al. 2004) and has already been proven useful for the study of comet 81P/Wild 2 samples (Sandford et al. 2006).

We describe below the results of STXM μ-XANES analyses performed on organic-containing particles extracted from cometary particle tracks identified in the aerogel tiles of the Stardust particle collector tray. A very cursory discussion of these analyses has been included in a recent report from the Organics subteam of the Principal Examination Team (PET) (Sandford et al. 2006). The emphasis of the present paper is to provide more detail on the experimental methods and greater in depth discussion regarding the implications of the data.

METHODS AND MATERIAL

Particle Extraction and Sectioning

Microscopic imaging was used to identify particles along obvious impact tracks. For the analysis of the track itself, the methodology involved first isolating an entire track into a small wedge-shaped volume of aerogel; referred to as a "keystone," that completely contains the track of the terminal dust particle. The particles were then extracted from the aerogel using disposable, pre-cleaned glass needles and computer-controlled micromanipulators (Westphal et al. 2004). For additional details regarding the particle extraction methods, please refer to Zolensky et al. (2006).

Extracted comet 81P/Wild 2 grains were transferred to either molten high-purity S or uncured electron microscopy–grade sectioning epoxy for embedding prior to sectioning. As will be shown below, it is worthwhile in studying both epoxy and sulfur-embedded particles. Samples were sliced into sections 100–140 nm thick with an ultramicrotome equipped with a diamond knife. The sections were floated onto ultrapure water and transferred to amorphous C or SiO-supported Cu transmission electron microscopy (TEM) grids. In the case of the S embedded samples, sulfur was sublimed prior to analysis under vacuum. Sulfur is an ideal embedding medium for the purpose of avoiding the complexity of co-mingling of organic matter in the samples with insoluble epoxy (typically composed of polymerized diphenylol propane) normally used for ultramicrotomy. Sulfur beads containing the samples were attached to a sample-holding bullet using cyanoacrylate. To evaluate the potential for cyanoacrylate contributing to spectral contamination and hindering sample analysis, sulfur beads devoid of sample were prepared in the same manner. No evidence has been observed that cyanoacrylate penetrated the S bead during subsequent TEM investigation of the sample-free S slices. Significantly, electron energy-loss spectroscopy (EELS) spectra acquired from the S test slices do not show any evidence of the pronounced nitrile absorption peak characteristic of cyanoacrylate. The samples and their designations, sectioning media, and associated mineralogy are summarized in Table 1.

Table 1. Sample designations for comet 81P/Wild 2 particles analyzed in this study.

Sample ID	Generic	Track	Grain	Mount	Medium	Fe-present	Silicate
1	FC12	16	1	10	Epoxy	ND	Trace
2	C2054	35	16	4	Epoxy	Yes	Yes
3	C2115	22	1	5	Sulfur	ND	Yes
4	C2054	35	10	10	Sulfur	ND	Yes
5	C2054	35	8	8	Sulfur	ND	Yes
6	C2044	36	1	1	Sulfur	Yes	Yes
7[a]	FC9	13	1	8	Sulfur	ND	Yes
8[a]	FC9	13	1	8	Sulfur	ND	Yes
9	C2115	22	1	5	Sulfur	ND	Yes

[a]These are different slices of the same particle, with significantly different cross sections and positions on the grids.
ND = not detected.

Scanning Transmission X-ray Microscopy and μ-XANES on Carbon, Nitrogen, and Oxygen 1s Absorption Edges

The STXMs employed in this principal examination phase of the Stardust organics analysis are located at beam lines 5.3.2 and 11.3.2 at the Advanced Light Source (ALS), Lawrence Berkeley Laboratory and beam line X1A at the National Synchrotron Light Source (NSLS), Brookhaven National Laboratory. The STXMs at beamlines (BL) 5.3.2 and 1l.0.2 at the ALS are built from very similar designs. They differ, however, in the means by which soft X-rays are generated. BL5.3.2 employs a bending magnet providing a useful photon range spanning ~250 to 700 eV with a photon flux of 10^7 photons/s. Energy selection on BL5.3.2 is performed with a low dispersion spherical grating monochromator affording an energy resolution of 5000. BL11.0.2 utilizes an elliptical polarization undulator, with gap correlated with monochromator position, that provides a wider energy range: 80 eV–2100 eV with a photon flux of 10^{12} to 10^{13} photons/s (10^9 photons/s with full spatial resolution) and employs a monochromator that can provide energy resolution up to 7500.

The STXM at beamline X1A also uses an undulator for X-ray generation. However, unlike beamline 11.0, there is no STXM control of the undulator gap; rather, the X1A undulator is intrinsically detuned, providing sufficient band width to span a given ionization edge region, e.g., the C-XANES region from ~280 to 320 eV. Energy selection is performed with a spherical grating monochromator, higher order energy contamination is removed with order sorting mirrors, and X-ray microfocusing is performed with Fresnel zone plate optics (Jacobson et al. 1991).

All of the STXMs utilize Fresnel zone plate optics providing a theoretical spot size of 30 nm; in optimum cases smaller structures (~15 nm) can be resolved. Maximum scanning rates for both BL5.3.2 and 11.0.2 is 12 Hz, with a scanning range of 4000 × 2000 pixels covering a region up to 20 × 4 mm, with a minimum step size 2.5 nm. Sample position precision during spectra acquisition is better than 50 nm (controlled by laser interferometry) (Kilcoyne et al. 2003).

C-, N-, and O-XANES spectra were typically acquired using a multi-spectral imaging method ("Stacks," Jacobsen et al. 2000). The "Stacks" method relies on creating a highly aligned hyper-spectral data cube of x by y pixilated images acquired over a range of energies that span a given XANES region. In the fine structure regions of the near edge, the energy step size (ΔE) employed typically was 0.1 eV; in the less featured pre-edge and post-edge regions, energy steps of 1–2 eV are typically sufficient for spectral resolution.

RESULTS

Carbon XANES

C-XANES reveals the presence and abundance of various organic functional groups via the detection of characteristic absorption features in the near edge (pre-ionization) region of the X-ray absorption spectrum. In general, absorption at the lowest energies (~285.0 eV) is well-described by photo-excitation of carbon 1s, electrons to low-energy, unoccupied, π* orbitals of alkenyl and aromatic species (C and H substituted). Carbon substitution with more electronegative atoms, e.g., N and O, results in shifts to higher excitation energies, e.g., 288.5 eV in the case of carboxyl 1s-π* transitions (Urquhart and Ade 2002). Saturated carbon, i.e., methyl and methylene, also exhibit relatively intense absorption in the near-edge region (e.g., Hitchcock and Mancini 1994), where the electronic transition for saturated carbon involves photoexcitation of a 1s electron to a hybrid state involving mixing of a 3p Rydberg state with a σ* C-H orbital, commonly identified as a 1s-3p/σ* transition (Stöhr 1991). The intensity of the 1s-3p/σ* absorption is a strong function of the number of H's per carbon, i.e., this transition is most intense for methyl groups, and very weak for methine carbon. The energy of the 1s-3p/σ* transition is also effected by the electronegativity of bonded species, e.g., N and O, this leads to a shift of the 1s-3p/σ* transition to higher energies, e.g., from ~287.8 eV for simple hydrocarbons up to 289.5 eV for alcohols (Hitchcock and Mancini 1994). For most organic compounds, the absorption spectrum at energies exceeding the carbon 1s ionization edge (i.e., ~290.8 eV for benzene;

Table 2. Various C-, N-, and O-XANES transitions and associated functional groups.

Photon energy	Transition	Functional group	
C-XANES assignments[a]			
283.7	1s-π*	C=C*-C=O,	Quinone
285.2	1s-π*	C=C*-H,C,	Aromatic and olefinic carbon
286.1–286.3	1s-π*	C=C*-C=O	Aryl, vinyl-keto
286.5	1s-π*	C=C-C*=O	Vinyl-keto
286.7–286.9	1s-π*	C*≡N	Nitrile
287.2	1s-π*	C=C*-OR	Enol
287.3–288.1	1s-3p/s*	CHx-C,H	Aliphatics
287.9–288.2	1s-π*	NHx(C*=O)C	Amidyl
288.4–288.7	1s-π*	OR(C*=O)C	Carboxyl
288.9–289.8	1s-π*	NHx(C*=O)NHx	Urea
289.3–289.5	1s-3p/s*	CHx-OR	Alcohol, ether
290	1s-π*	NHx(C*=O)OR	Carbamoyl
290.3–296	1s-π*	RO(C*=O)OR	Carbonate
N-XANES assignments			
398.8	1s-π*	C=N*	Imine
399.8	1s-π*	C≡N*	Nitrile
401.9	1s-π*	N*Hx(C=O)C	Amidyl
402.1–402.3	1s-3p/s*	C-N*Hx	Amine, pyrrole
402.5–402.6	1s-3p/s*	C-N*Hx	Amino
403	1s-3p/s*	CO- N*Hx	Urea
O-XANES assignments			
531.2	1s-π*	C=O*	Ketone
532.0	1s-π*	O-C=O*	Carboxyl
534.4	1s-3p/s*	CHxO	Alcohol, ether
534.9	1s-3p/s*	C=C-O*	Enol

[a]These assignments are derived from both the gas phase electron energy loss spectral database of simple compounds Hitchcock and Macinini (1994), updated to the present at the Hitchcock group of McMaster University (http://unicorn.mcmaster.ca), as well as the polymer STXM database supported by the Harald Ade and the Polymer STXM group at NSCU (http://www.physics.ncsu.edu/stxm/polymerspectro).

Hitchcock and Mancini 1994) consists of very broad spectral features, corresponding to highly delocalized excited states (in some cases referred to as 1s-σ* virtual state transitions [Stöhr 1991]). Representative assignments of functional groups with characteristic absorption energies are presented in Table 2.

Commonly, the samples analyzed in this particular study were intimately associated with silica, likely derived from aerogel, and in many cases embedded in epoxy for sectioning (see Table 2 for sample designations and descriptions). In order to acquire C-XANES spectra from samples that were embedded in epoxy, it is necessary to subtract the epoxy C-XANES spectrum from the particle spectrum. This is easily done, due to the fact that the epoxy spectrum exhibits extremely sharp, characteristic, absorption bands at 285.15 and 287.2 eV, respectively. Analysis of the derivative of the combined particle plus epoxy spectrum clearly reveals the contribution due to the epoxy allowing for an objective determination of the fractional contribution of pure epoxy to the total spectral intensity. In the case of silicate intermingled with organics, there exists no overlapping fine structure to worry about as the tail of the silicon (2p, L edge) absorption passes smoothly under the carbon, nitrogen, and oxygen k-edges. For presentation purposes, a simple baseline correction is all that is necessary. In order to obtain elemental ratios of N/C and O/C, however, a precise estimate of the contribution of silicon absorption must be determined as is described below.

C-XANES spectra of eight organic samples extracted from the Stardust aerogel collector are presented in Fig. 1. In addition, representative C-XANES spectra of an anhydrous IDP (L2011R11; Flynn et al. 2003), insoluble organic matter (IOM) from a very primitive chondritic meteorite, EET 92042 (CR2; Cody and Alexander 2005; Busemann et al. 2006), and a moderately thermally altered chondrite, Allende (CV3; Brearley and Jones 1998) are also included for comparison. It is immediately clear that the majority of organic samples extracted from the Stardust aerogel collector are complex, with C-XANES spectra showing the presence of carbon in a range of electronic environments. One exception is particle 1 (Table 2), which exhibits a relatively simple C-XANES spectrum dominated by a broad peak centered at ~289.3 eV (F, Fig. 1). Intensity in this energy range likely signifies the presence of abundant alcohol and/or ether moieties (Hitchcock and Mancini 1994).

Samples 2 and 3 share a chemical characteristic not observed in the other samples analyzed—a very intense peak at 288.2 eV (D, Fig. 1) that most likely corresponds to

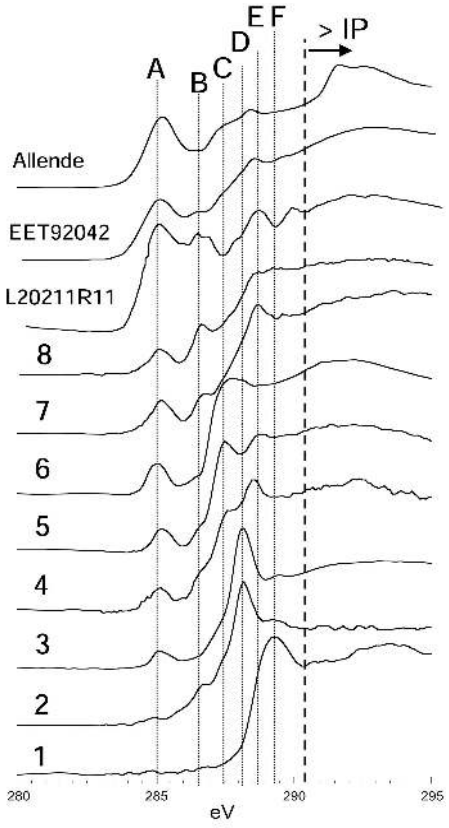

Fig. 1. A stack plot of C-XANES spectra obtained of organics associated with particles extracted from the Stardust aerogel collector (sample numbers 1–8; Table 1). Included for comparison are a spectrum of an anhydrous IDP (L2011R11) insoluble organic matter isolated from a CR2 meteorite (EET 92042) and a CV3 meteorite (Allende). Peaks corresponding to specific functional groups are highlighted with the letters A–F; where A (~285 eV) corresponds to a 1s-π* transition associated with aromatic or olefinic carbon; B (~286.5 eV) corresponds to a 1s-π* transition associated with oxygen substituted double-bonded carbon, e.g., enolic carbon; C (~287.5 eV), corresponds to a 1s-σ*/3p transition associated with methyl groups; D (~288.2 eV) corresponds to a 1s-π* transition associated with carbonyl carbon in amide moieties; E (~288.7 eV) corresponds to a 1s-π* transition associated with carbonyl carbon in carboxyl moieties; and F (~289.4) corresponds to a 1s-σ*/3p transition associated with alcohol/ether moieties. The approximate position of the carbon 1s ionization threshold is designated with a dashed line (labeled IP).

a carbonyl group in an amide moiety (Table 2). This assignment is supported by N-XANES as is described below. Particle 2 also exhibits a well-developed shoulder at ~286.5 eV and a weak peak at 285.2 eV (B and A, respectively). Peak A corresponds to sp^2 bonded carbon substituted with either C or H, i.e., olefinic and/or aromatic carbon hydrocarbon. Note that all of the samples (with the exception of particle 1) exhibit some intensity at ~285 eV (A, Fig. 1) signifying the presence of minor amounts of either olefinic or aromatic carbon; the relative concentration of such carbon in any of the samples, however, is considerably less than that observed in either the IDP or the chondritic organic samples (Fig. 1).

The peak at 286.5 eV (B, Fig. 1) likely indicates the presence of vinyl-keto groups (Hitchcock and Mancini 1994). Absorption at this energy is observed to varying extents in all of the samples (excluding 1), and is particularly intense in samples 7 and 8. Note that both the IDP, L2011R11, and the chondritic IOM from EET 92042 also exhibit significant intensity in this region. Very commonly, vinyl-keto groups observed in C-XANES spectra from both terrestrial and extraterrestrial organics actually form during acquisition as a consequence of X-ray–induced damage. Specifically, labile polyol moieties (e.g., polysaccharides) suffer OH elimination reactions through collision with energetic secondary electrons generated by the photoabsorption process (Cody 2000). The observation of this band in the comet 81P/Wild 2 organics, therefore, provides indirect evidence for the presence of poly-hydroxylated moieties (for example, sugar derivatives). Finally, it is also noted that both imine and nitrile carbon exhibit 1s-π* transitions in the range 286.7 to 286.9 eV (Table 2) and their presence cannot be ruled out based on C-XANES alone. N-XANES, however, (see below) does not support the presence of imine or nitrile in sufficient quantities to be detected in the C-XANES spectra amidst the other functional groups.

Several of the samples (e.g., 4, 5, and 6) exhibit considerable intensity at 287.5 eV (C, Fig. 1). Particle 5, for example, exhibits a distinct peak at this energy. Absorption in this energy range generally points to aliphatic moieties (Table 2), although the energy of peak C is on the low side for typical aliphatic hydrocarbons. The methyl groups of ethane, for example, exhibit a relatively sharp peak at 287.9 eV corresponding to the 1s-3p/σ* transition (Stöhr 1991), methyl groups decorating aromatic rings exhibit a characteristic peak at 288.3 eV (Hitchcock and Mancini 1994). Interestingly, methyl groups in tetramethyl-silane exhibit their 1s-3p/σ* transition at 287.3 eV (Hitchcock and Mancini 1994), suggesting that the peak at 287.5 eV may be due to methyl-groups decorating silicon. Solid-state ^{29}Si nuclear magnetic resonance (NMR) spectroscopy of bulk aerogel reveal the presence of silicone moieties and solid state ^{13}C NMR spectroscopy show that the predominant form of carbon in aerogel is methyl-silica moieties (Cody, unpublished data). A C-XANES spectrum of silicone oil is presented in Fig. 2, revealing a sharp peak at 287.5 eV corresponding to CH_3-Si groups. Thus, at least some of the carbon in samples 4, 5, and 6 may be organic carbon intrinsic to bulk aerogel. It is noted that C-XANES analysis of silica-rich regions of some of the samples yielded spectra that are very similar to that of silicon oil (Fig. 2) and is consistent with what is expected in terms of the intrinsic background carbon signal associated with the aerogel.

Samples 7 and 8 are different ultrathin sections acquired from the same particle (Table 1), hence it is expected that they share similar chemistry. Among the samples analyzed so far, these two samples exhibit the greatest amount of olefinic and/

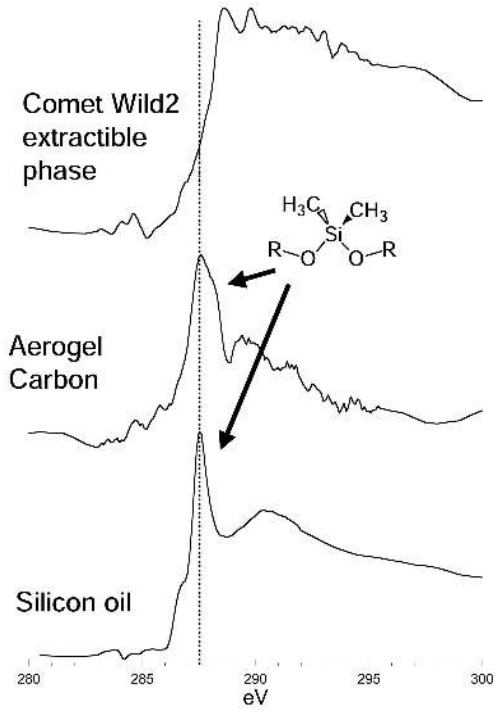

Fig. 2. C-XANES spectra of pure silicone oil (bottom), a highly silica-rich region (middle), and the soluble phase that was extracted by the epoxy from embedded particles (top). Note that the low signal-to-noise exhibited in silica-rich region spectrum (middle) is due to the very low carbon content. The dominant functionality in both the silicone oil and the silica-rich regions are silica bonded methyl groups. The epoxy soluble material is clearly not silicone oil or aerogel.

or aromatic hydrocarbon, i.e., intensity at 285 eV, as well as the most intensity at 286.6 eV (A and B, Fig. 1, respectively). In this regard, samples 7 and 8 bear the greatest chemical similarity to the anhydrous IDP, L20211R11, and the primitive chondrite IOM, EET 92042 (CR2), in terms of the types and relative abundance of functional groups present.

In the course of analyzing the samples that were embedded in liquid epoxy (prior to sectioning), it became immediately apparent that there exists a carbonaceous phase in these samples that is soluble and extracted by the liquid epoxy. During curing, this soluble phase migrates from the particle into the surrounding liquid epoxy. The presence of such a soluble phase has been observed in every particle analyzed so far that was embedded in epoxy; an example is presented in Fig. 3. The soluble phase extracted from the silicate-rich particle in Fig. 3a is contrast-resolved from epoxy particularly well at energies just below the C-XANES region, e.g., 280 eV, and on the peak of O-XANES absorption, e.g., 540 eV. In Fig. 3b, a C-XANES spectrum of pure epoxy is presented along with a C-XANES spectrum of the soluble phase obtained by subtracting the pure epoxy C-XANES spectrum from the combined epoxy + soluble phase spectrum. We find that ~10% of the intensity of the dark region in Fig. 3a corresponds to the presence of carbon, that is not epoxy, and is associated with an apparently soluble phase extracted from the embedded particle.

The C-XANES spectrum of the soluble organic phase is expanded vertically in Fig. 2 and presented with a C-XANES spectra of pure silicone oil (Fig. 2, bottom) and that of silicone moieties intrinsic to the aerogel. It is clear from this C-XANES spectrum that the soluble phase is neither silicone oil nor aerogel, rather the dominant organic species includes carboxyl and alcohol/ether moieties along with minor olefinic/aromatic and other species. At this point we cannot attribute this phase to any obvious contaminant and include this extractable phase in subsequent discussions as if it were a genuine comet 81P/Wild 2 organic phase.

Nitrogen XANES

Nitrogen XANES provides complementary information to the C-XANES data, revealing the distribution of nitrogen containing functional groups. Characteristic energies corresponding to nitrogen in various unsaturated and saturated moieties are presented in Table 2. Unsaturated nitrogen species are readily distinguished, as there are significant shifts in energy corresponding to imine and nitrile 1s-π^* transitions (Table 2). Similarly, the 1s-3p/σ^* transitions of amino NH may be distinguished from aliphatic and aromatic amine and from pyrrolic NH. Similar to C-XANES behavior of CH_x moieties, the intensities of the NH_x 1s-3p/σ^* transitions are proportional to the number of hydrogen atoms, i.e., primary amines are expected to exhibit considerably more intense 1s-3p/σ^* transitions than secondary and tertiary amines.

Given that the nitrogen abundance is a fraction of that of carbon, the signal-to-noise (S/N) of the N-XANES spectra is generally much worse than that of C-XANES. Only the samples that provided sufficient S/N N-XANES spectra are presented in Fig. 4, along with N-XANES spectra for the IDP L20211R11 and chondritic organic matter from EET 92042 (CR2) and Allende (CV3).

Similar to what was observed in the C-XANES data presented in Fig. 1, considerable variation in nitrogen chemistry is observed across the various samples analyzed (Fig. 4). The generally broad N-XANES spectra also reveal that nitrogen speciation within most of samples is relatively complex. For example, samples 1, 5, and 8 exhibit nearly featureless N-XANES spectra with absorption growing continuously from ~398 eV up to the ionization threshold (IP) at ~405 eV (Henke et al. 1993). Given that the absorption intensity peaks near the ionization threshold strongly suggests that the dominant nitrogen functional groups are amino, urea, and carbamate moieties, with lesser amounts of imine, nitrile, and amido nitrogen (Fig. 4).

Samples 2 and 3 exhibit better resolved fine structure in the their respective N-XANES spectra (Fig. 4) as compared

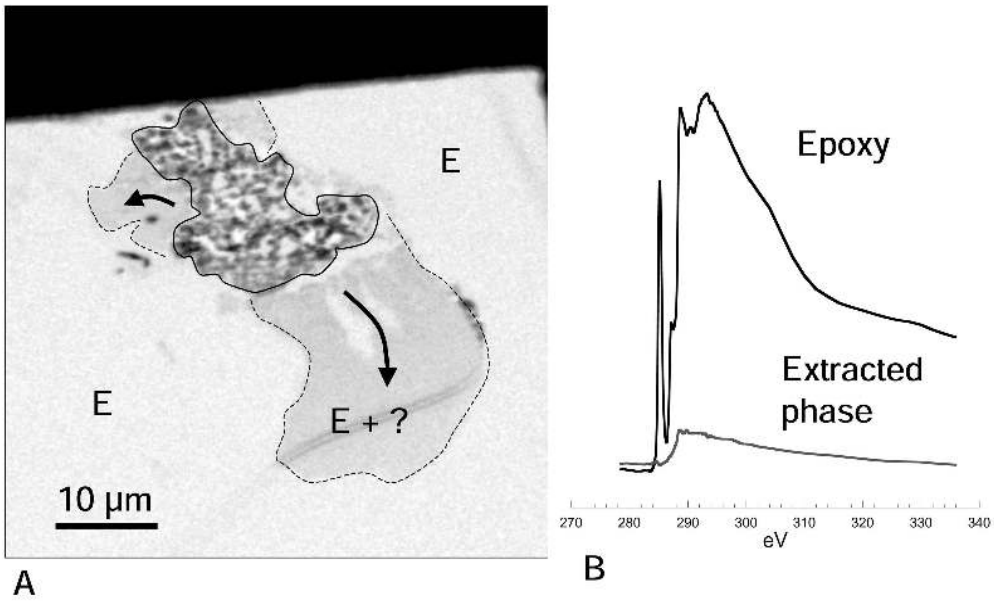

Fig. 3. a) X-ray image of a particle from track 35, grain 16, (sample 2) acquired at 280 eV, just below the carbon 1s XANES region. Note the particle, largely granular and silica-rich (outlined with a solid line) is embedded in epoxy (E). Highlighted with dashed lines is a region of some other organic phase that was extracted by the liquid epoxy from the particle (E + ?). b) C-XANES spectra of the epoxy and the soluble phase obtained by subtraction of epoxy from the spectrum acquired in the E + ? field. The extracted phase constitutes ~10% of the carbon contributed by the epoxy.

with the other samples, meteorite IOM, and IDPs. In particular, a relatively sharp peak at 401.4 eV (I, Fig. 4) dominates the spectrum of particle 3. The C-XANES spectra of these two samples are similarly dominated by a single sharp peak at 288.2 eV (D, Fig. 1) that likely corresponds to a 1s-π* transition of a carbonyl (Urquhart and Ade 2002). Assignment of the 401.4 eV feature to amido nitrogen, therefore, appears reasonable, even though a pure compound study places the amido-N absorption at ~401.9 eV (Hitchcock and Mancini 1994; Table 2). It is also noteworthy that relative to the other samples, samples 2 and 3 exhibit weaker intensity in the region around 402.3 eV (J, Fig. 4) indicating proportionally less amine and amino functionality. Particle 2 exhibits clearly defined intensity in the 399 to 400 eV (G and H, Fig. 4) energy region supporting the presence of some imine and nitrile N. Nitrile N exhibits a very intense 1s-π* absorption band relative to the ionization cross section. This means that the intensity at ~400 eV, although most likely indicative of the presence of nitrile, actually reflects only a low concentration (likely less than ~5%) relative to the other N-bearing species.

Comparing the N-XANES spectra of these organic samples obtained from particles extracted from the Stardust aerogel collector with that derived from the anhydrous IDP L2011R11 and chondritic organic matter from EET 92042 (CR2) and Allende (CV3) reveals some similarities. The N-XANES from L20211R11 and EET 92042 (CR2) are similar, clearly exhibiting intensity that could be ascribed to the presence of imine/nitrile (G and H, ~399–400 eV) as well as amido-N (J, ~401.4–401.9 eV). Similar to samples 2 and 3; L2011R11 exhibits a valley in the spectral region where amine and amino nitrogen are expected; EET 92042 (CR2) exhibits somewhat greater intensity in this region. At least superficially, the N-XANES spectrum of particle 2 appears similar to that of L2011R11, whereas the N-XANES spectrum of particle 5 shares greater similarity with EET 92042. Samples 1 and 8 exhibit similar N-XANES spectra that differ from the other samples as well as the IDP and meteoritic IOM by virtue of minimal nitrile intensity (A, Fig. 4). In general, it can be said that the N-XANES spectra for all of these organic samples indicate a wide range of nitrogen containing functional groups with considerable variation in the relative abundance of these nitrogen containing functional groups.

Oxygen XANES

While O-XANES of comet 81P/Wild 2 organics were acquired, they are not discussed in any detail here. This is because there tends to be considerably less chemical information obtained from the O K edge beyond the ratio of single to double bonded oxygen. This ratio, while a useful piece of information, is unreliable in many of the samples due to the contribution of a relatively high oxygen background signal derived from associated silica. As is discussed below, however, O-XANES data are still useful for the purpose of deriving quantitative O/C ratios.

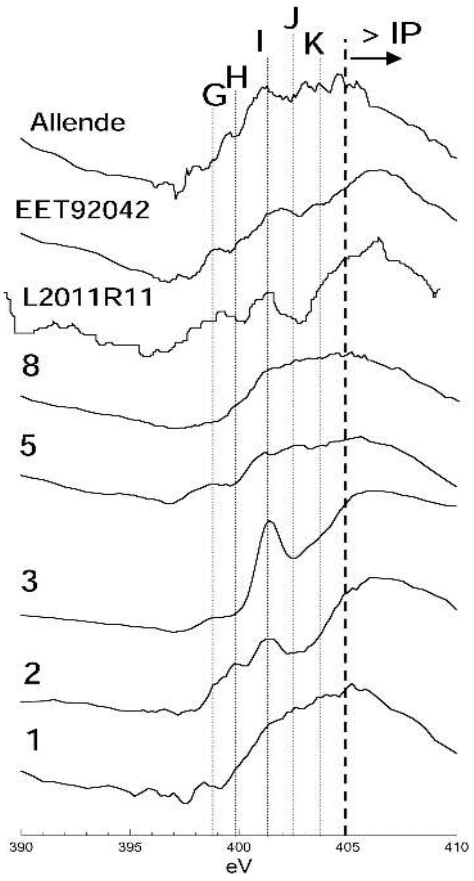

Fig. 4. N-XANES spectra obtained of organics associated with particles extracted from the aerogel collector (samples 1– 8; Table 1). Included for comparison are a spectrum of an anhydrous IDP (L2011R11, 2), and insoluble organic matter isolated from meteorites, CR2 (EET 92042) and CV3 (Allende). Peaks corresponding to specific functional groups are highlighted with the letters G–K. G (~399 eV) corresponds to a 1s-π* transition associated with imine nitrogen (C=N*); H (~400 eV) corresponds to a 1s-π* transition associated nitrile nitrogen (C≡N*); I (~401.4 eV) corresponds to a 1s-π* transition associated with amidyl nitrogen (O=C-N*); J (~402.5 eV) corresponds to a 1s-σ*/3p transition associated with amino nitrogen; and K (~403.5 eV) corresponds to a 1s-σ*/3p transition associated with urea nitrogen. The approximate position of nitrogen's 1s ionization threshold is designated by a dashed line (labeled IP).

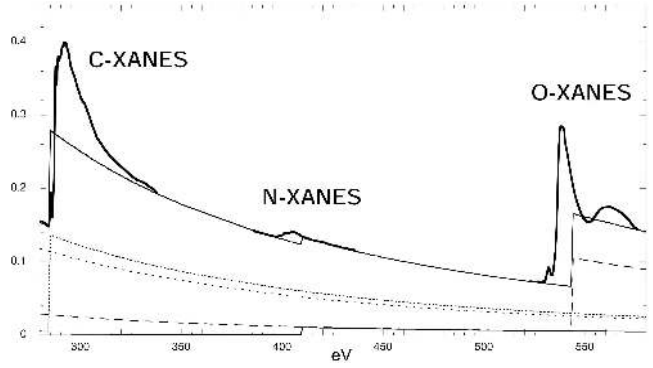

Fig. 5. An example of a computational fit of C-, N-, and O-XANES spectra of a cometary organic solid (sample 5; bold solid line). Atomic absorption cross sections are used directly, where the contribution from carbon is included with close spaced fine dashed line, nitrogen (solid line), oxygen (broad dashed line), and silica (fine open spaced dashed line). The sum of these provides the quantitative fit resulting in a precise determination of atomic C, N, O, and Si, e.g., N/C = 0.12 ± 0.01, O/C = 0.28 ± 0.03 (corrected for oxygen associated with silica), and Si/C = 0.51.

Elemental Abundances

While the near-edge fine structure of the carbon, nitrogen, and oxygen 1s absorption spectra provide valuable information regarding the presence of specific organic functional groups, the overall intensity of absorption spanning both below and well above a given ionization edge provides a quantitative measure of the atomic abundances of carbon, nitrogen, oxygen, and silica. This is because for the lower Z elements absorption in the soft X-ray range is dominated by the photo-ionization cross sections, whereas atomic scattering is very weak (Stöhr 1991). In order to obtain quantitative estimates of N/C and O/C, we employ the mass absorption coefficients of Henke et al. (1993) and fit our C-, N-, and O-XANES data directly.

In the case where epoxy is intimately commingled with the Stardust organics, epoxy N- and O-XANES must obviously also be subtracted in order to obtain pure phase N/C and O/C ratios. As the N/C and O/C ratio of epoxy is constant and subtraction of epoxy carbon from Stardust carbon is accurate to within the limit of signal to noise, subtraction of epoxy does not add any significant uncertainty to the sample N/C and O/C. On the other hand, the presence of commingled silicate is a major source of uncertainty in the organic O/C ratio.

The majority of samples analyzed in the present study are intimately associated with silicate derived primarily from the aerogel. Silicon exhibits relatively intense absorption across the spectra range 200 to 600 eV due primarily to photo-absorption by the 2p and 2s electronic levels (Thompson et al. 2001). The presence of silicate obviously presents a particular problem with determining the oxygen content of the organic samples. The estimated oxygen content will be the sum of both silicate and the organic matter. If the fraction of non-bridging oxygen (NBO) intrinsic to the aerogel is known then one can correct the oxygen content based on the silica content. For example, if NBO = 0 as in the case of quartz than one silicon is balanced with twice as much oxygen. As a product of solid-state ^{29}Si NMR analysis of bulk aerogel (Cody, unpublished data), the fraction of NBO has been established for Stardust aerogel yielding an average formula for the aerogel of $SiO_{2.13}$. Provided that the O/Si ratio did not change upon particle capture, this ratio allows us to obtain a precise estimate of the organic O/C.

Table 3. Elemental chemistry derived for comet 81P/Wild 2 samples via C, N, and O-XANES.

Sample ID	O/C	±	N/C	±	Si/C	S/C[a]	Fe/C[b]
1	0.67	0.02	0.07	0.01	0.02		
2	0.11	0.01	0.23	0.03	0.13		
3	0.18	0.02	0.24	0.03	0.13		
4	0.25	0.03	0.07	0.02	0.52		
5	0.28	0.03	0.12	0.01	0.51		
6	0.27	0.03	NA	–	–	–	1.15
7	0.19	0.01	0.07	0.01	0.19		
8	0.22	0.01	0.12	0.01	0.17		
L20211R11	0.49	0.06	0.12	0.01	0.69	–	–
Sol. Phase	0.59	0.05	0.12		1.06	0.92	
Bulk aerogel	–	–	–	–	20–100[c]		

[a]It is possible that in the case of the soluble phase baseline shift could also be due to presence of sulfur instead of silica.
[b]Sample 6 is closely associated with an iron-rich particle (not silica).
[c]These values were determined by solid state ^{13}C and ^{29}Si NMR (Cody, unpublished data).
NA = not analyzed.

An example of a typical fit to the combined C-, N-, and O-XANES data for sample 5 is presented in Fig. 5. The individual contributions from C, N, O, and Si are summed to provide the best fit of the photo-absorption cross section. Note that at both the carbon and oxygen edges there exists considerable absorption intensity above the ionization edge that exceeds that predicted based on the Henke et al. (1993) data. This intensity results from the so called σ* shape or Feshbach resonances (Stöhr 1991). The data presented in Fig. 5 are derived from a total particle analysis and indicate an elemental formula of $C_{100}N_{13}O_{154}Si_{57.5}$; yielding an organic O/C of 0.31 assuming and O/Si of 2.13.

The edge structure of the epoxy extractible phase of carbon (Figs. 2 and 3) requires a contribution from an element other than C, N, and O in order to account for all of the absorption. In Table 3, we calculate the total absorption, including the contribution of either silicon or sulfur and find that in either case, a relatively high Si/C or S/C is required to fully account for the absorption characteristics. The elemental ratios O/C, N/C, and Si/C are presented in Table 3 and in Fig. 6. Also included in Fig. 6 are elemental ratios representative of type 1, 2, and 3 chondritic IOM (Alexander et al. 2007) and elemental data derived for the anhydrous IDP L2011R11 (Feser et al. 2003). In order to obtain an estimate of O/C from the published data obtained for the whole particle of anhydrous IDP L2011R11, it was necessary to estimate the degree of polymerization of the silicates in the GEMS (see review by Rietmeijer 1998 and references therein) as well as the modal abundance of enstatite. As it is not well known what the relative modal abundances of enstatite and GEMS are in this particular IDP, we considered a wide range spanning from 30% to 70% enstatite, this model uncertainty provides the greatest uncertainty in the elemental ratios presented in Table 3 and Fig. 6.

It is interesting that the elemental chemistry of the anhydrous IDP L2011R11 is richer in oxygen than the majority of samples analyzed in this study. If anhydrous IDPs do constitute remnants of cometary matter (Brownlee et al. 1995; Rietmeijer 1998), then it may be possible that the relative reduction in oxygen evident in the organic samples retrieved from the aerogel is evidence of alteration during the energetic phase of particle capture. It is worth noting, however, that while this IDP clearly has not suffered any aqueous alteration since its formation, it has undergone mild thermal processing during atmospheric entry (Flynn et al. 2003; Keller et al. 2004). Furthermore, the C-XANES spectrum of L2011R11 reveals considerable intensity at 286.5 eV, which is possibly indicative of significant secondary electron damage (Cody 2000).

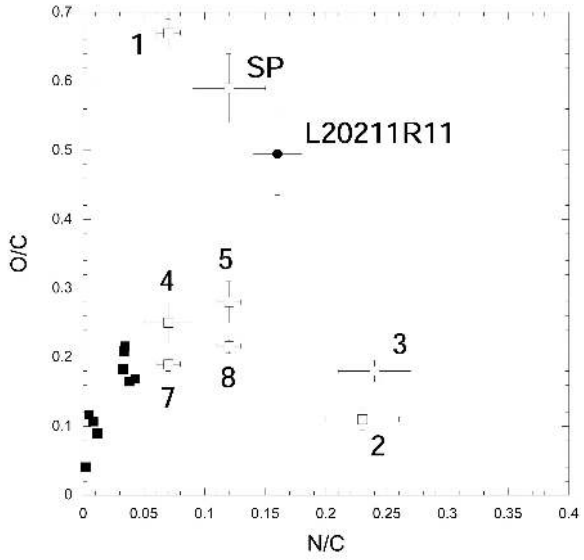

Fig. 6. Atomic N/C versus O/C derived from C-, N-, and O-XANES of organics associated with particles extracted from the Stardust aerogel collectors (□). Included are elemental data for meteoritic organic matter isolated from types 1, 2, and 3 chondrites (■) and the anhydrous IDP L20211R11 (●).

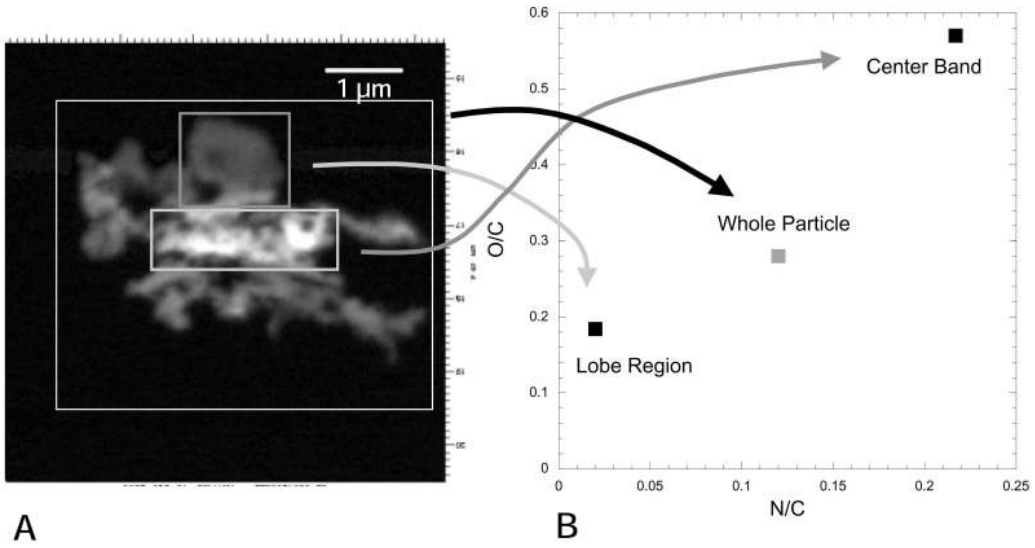

Fig. 7. a) An optical density image on the carbon (1s) absorption edge of sample 5 (track 35, grain 8, mount 8). Note that the significant variations in optical density could be due to variations in particle density or chemical heterogeneity. b) Elemental data (N/C and O/C) from the "lobe region" and the "center band" reveal that the variation in optical density observed (left) reflects significant chemical heterogeneity within the sample.

In general, the comet 81P/Wild 2 samples analyzed so far are distinct in terms of their respective O/C and N/C ratios from primitive chondritic organic matter. Perhaps more significantly, however, it is clear that the cometary organics exhibit a spectacularly large degree of variation in their elemental chemistry. Is this variation a primary feature of the cometary organics or a secondary feature overprinted during the energetic phases of sample capture? Deriving an unequivocal answer to this question will likely require considerably more analyses. It should be noted, however, that the scatter in the range of N/C and O/C is not what would be expected if a single cometary organic precursor was chemically evolved to various degrees by thermal transformation.

The trajectory of the change in elemental ratios with progressive thermal transformation of terrestrial kerogens is well established (van Krevelan 1992). What is observed is large losses in oxygen, followed by less significant loses in nitrogen. The macromolecular structure of terrestrial kerogen must differ enormously from that of extraterrestrial organic solids. However, neither the oxygen and nitrogen containing functionalities in the cometary organic matter are particularly exotic and considering a single primitive, cometary, end-member one would expect the signature of thermal modification to exhibit more covariance between O/C and N/C (e.g., that which is observed for meteoritic organics, Alexander et al. (2007), not the scatter observed in Fig. 6.

The spectacular interparticle heterogeneity detected in this preliminary analysis of comet 81P/Wild 2 organics is striking as it suggests that there may not be a unique cometary organic precursor. Rather, intrinsic heterogeneity of the organic particles may be the rule and is consistent with the wide range of heterogeneity observed mineralogically (Brownlee et al. 2006, Zolensky et al. 2006), chemically (Flynn et al. 2006; Sandford et al. 2006), and isotopically (McKeegan et al. 2006).

The variation in the types of O- and N-bearing functional groups is similarly intriguing, as there exists no simple means of transforming (at least via a fast thermal process as might have occurred during aerogel capture) the organic solids detected in some of the particles into that observed in other particles. Rather, the spread in chemistry may suggest that the particles captured by the Stardust spacecraft cannot be linked to a common precursor. This raises the interesting question as to whether the organic solids extracted from the aerogel collector universally represent solids that formed via cometary processes or whether some of the solids could have formed from reactive low molecular weight precursors either during or after capture. It is notable in this regard, that particle 1 (Fig. 1; Table 1) stands out from the others with functional group characteristics that are similar to that expected in simple condensation polymers such as poly[oxymethylene] derived from formaldehyde and urea-formaldehyde-derived polymeric resins.

Intra-Particle Heterogeneity

One of the intriguing aspects of interplanetary dust samples and meteoritic IOM is the submicron scale spatial heterogeneity evident both in terms of organic chemistry (e.g., Flynn et al. 2003) and in terms of isotopic abundances, e.g., H/D and/or $^{15}N/^{14}N$ (e.g., Keller et al.

2004; Busemann 2006). In this regard, it is interesting that while samples 7 and 8 (Table 1) were obtained from sequential sections of a single large particle, it is clear from the C-, N-XANES, and elemental data (Figs. 1, 3, and 6) that the chemical characteristics of samples 7 and 8 are not identical, suggesting that the organic solids captured by the Stardust mission may also be heterogeneous at a fine scale. Such sub-micron scale heterogeneity in comet 81P/Wild 2 organic samples is dramatically confirmed in the case of sample 5.

Recalling that all spectroscopic data was acquired via multi-spectral ("Stacks" imaging (Jacobsen et al. 2000), the C-, N-, and O-XANES data and the elemental data presented in Figs. 1, 4, and 6 constitute the sum (the average) of all pixels. This was done to optimize the signal to noise; and was originally justified because none of the samples exhibited evidence of heterogeneity. The exception to this is sample 5. An optical density image (on the carbon K edge) of sample 5 (Fig. 7a) reveals considerable variation in absorption intensity across the particle, with considerable intensity in the particle center. Variations in absorption intensity may be due to characteristics other than organic chemical heterogeneity. For example, variations in absorption may be due entirely to variation in carbon density or variation in the relative concentration of silica intermixed with organics. In the case of sample 5, the average the Si/C ratio is on the order of 0.52 (Table 3). Thus, the bright region in Fig. 7a may very well reflect increased silica. Analyzing only those pixels that correspond to the bright ("center") region in Fig. 7a and comparing these with the homogenous "lobe" region (Fig. 7a) reveals that the molar abundance of carbon in both regions is essentially the same, but the contribution to total absorption due to silica is very different (with a Si/C ratio of 0.51 for the "lobe" region and 0.88 for the "center" region); hence the apparent increased brightness in the optical density image (Fig. 7a). Given that the capture medium of the Stardust mission was low-density aerogel, it is not surprising that the organic samples would be intimately associated with silica.

Based on image contrast alone, therefore, the apparent chemical heterogeneity of sample 5 might only reflect variations in silica content. We find, however, that XANES spectroscopy (particularly on the nitrogen L edge) reveals considerable differences in the nitrogen and oxygen content within these two domains; i.e., Fig. 7b shows that the O/C and N/C of the "lobe" region is considerably less than that of the center region. The C- and N-XANES spectra of the "lobe" and "center" regions are presented in Figs. 8a and 8b. Whereas there are subtle differences in the C-XANES spectra of the two regions, the N-XANES differs considerably. In particular, it is clear that the nitrogen chemistry associated with the "center" region differs from that of that of the "lobe" region more than just in relative abundance. Whereas both the center and lobe regions exhibit intensity consistent with amido and amino nitrogen (I and J,

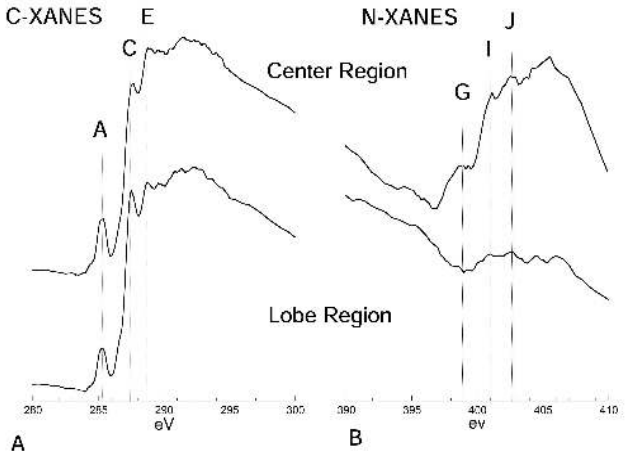

Fig. 8. a) C-XANES spectra of sample 5 "lobe" (bottom) and "center band" (top) revealing significant differences in the relative distribution of specific functional groups. b) N-XANES spectra of the same regions revealing significantly less abundant N in the "lobe" region (bottom) and considerable differences in the relative abundance of N functional groups. The obvious peaks corresponding to specific functional groups are identified as: A) C=C, 1s-π*, C) CH_3 1s-σ*/3p, D) O-C=O, 1s-π*, G-H) C=N and/or C≡N 1s-π*, I) amidyl 1s-π*, and J) amino N 1s-σ*/3p.

Fig. 8b), unsaturated nitrogen, e.g., imine and nitrile nitrogen (G, Fig. 8b), are nearly absent in the N-XANES spectrum of the "lobe" region.

The enormous difference in nitrogen content and variation in nitrogen chemistry across sample 5 is extremely interesting, and the origin and/or significance of this heterogeneity is not well understood at this point. It is worth noting that while in the case of sample 5 the high nitrogen content does correlate spatially with elevated silica, among all of the samples analyzed so far, there is no obvious correlation between high nitrogen and high silica. Samples 2 and 3, for example, have high N/C but relatively low silica contents. Sample 4 has a moderately high silica content, but low N/C. Clearly many more comet 81P/Wild 2 samples will have to been analyzed before the statistical significance of such heterogeneity, as well as an explanation regarding its origin, is determined.

CONCLUSIONS

The unique capability of STXM μ-XANES to interrogate small organic particles has helped to provide an informative view into the nature of cometary organics. All of the samples described in this paper exhibit highly complex organic structures composed a many different functional groups, in particular, a rich inventory of heteroatom bearing functional groups. Perhaps the most important aspect of these data is, however, the remarkable range in both elemental and corresponding organic functional group chemistry seen across the comet 81P/Wild 2 samples. Such a wide range in

chemistry, despite analysis of a relatively small set of particles, means that it is not yet possible to describe in any statistically significant way the average organic structure of comet 81P/Wild 2. At this stage there appear to be a least three distinct classes of organics associated with the Stardust samples analyzed here. These include 1) the relatively dense, moderately oxygen- and nitrogen-rich particles that share functional group similarity with organic matter derived from primitive carbonaceous chondrites (particles 4, 5, 7, and 8); and 2) a highly nitrogen-rich phase with moderate oxygen content (particles 2 and 3), and a highly oxygen-rich phase with moderate nitrogen content (particle 1 and the soluble phase).

It is clear from these preliminary studies that the organic chemistry manifested in the organic particles extracted from the Stardust aerogel collector is rich and highly variable. Considerably more analyses will be required before we can sort out 1) the possible chemical effects associated with high-velocity capture, 2) an explanation for the tremendous range in chemical composition, and 3) a statistically reliable picture of the state of organic matter in the comet Wild 2. This latter goal may be complicated by the possibility that some of the organic phases observed actually formed during and after capture through condensation polymerization of reactive low molecular weight species.

Acknowledgments—Financial support for these analyses was provided in part by NASA's Stardust Analysis, Astrobiology, Cosmochemistry, and Origins of the Solar System programs. During the Preliminary Examination period data were acquired at the Advanced Light Source, Lawrence Berkeley National Laboratory, beam lines 5.3.2 and 11, as well as the National Synchrotron Light Source, Brookhaven National Laboratory, beam line X1A. Each of these facilities are supported by the Department of Energy, Basic Energy Sciences program. Financial support for the individual beam lines is generously provided by the DOE, the NSF, and NASA.

Editorial Handling—Dr. A. J. Timothy Jull

REFERENCES

Alexander C. M. O'D., Fogel M., Yabuta H., and Cody G. D. 2007. The origin and evolution of chondrites recorded in the elemental and isotopic compositions of their macromolecular organic matter. *Geochimica et Cosmochimica Acta* 71:4380–4403.

Boyce K. C., Cody G. D., Fesser M., Knoll A. H., and Wirick S. W. 2002. Organic chemical differentiation within fossil plant cell walls detected with X-ray spectromicroscopy. *The Journal of Geology* 30:1039–1042.

Brearley A. J. and Jones R. H. 1998. Chondritic meteorites. In *Planetary materials,* edited by Papike J. J. Reviews in Mineralogy, vol. 36. Washington, D.C.: Mineralogical Society of America. 398 p.

Brownlee D. E., Joswiak D. J., Schlutter D. J., Peppin R. O., Bradley J. P., and Love S. G. 1995. Identification of individual cometary IDPs by thermally stepped He release (abstract). 26th Lunar and Planetary Science Conference. pp. 183–184.

Brownlee D. E., Tsou P., Aléon J., Alexander C. M. O' D., Araki T., Bajt S., Baratta G. A., Bastien R., Bland P., Bleuet P., Borg J., Bradley J. P., Brearley A., Brenker F., Brennan S., Bridges J. C., Browning N. D., Brucato J. R., Bullock E., Burchell M. J., Busemann H., Butterworth A., Chaussidon M., Cheuvront A., Chi M., Cintala M. J., Clark B. C., Clemett S. J., Cody G., Colangeli L., Cooper G., Cordier P., Daghlian C., Dai Z., D'Hendecourt L., Djouadi Z., Dominguez G., Duxbury T., Dworkin J. P., Ebel D. S., Economou T. E., Fakra S., Fairey S. A. J., Fallon S., Ferrini G., Ferroir T., Fleckenstein H., Floss C., Flynn G., Franchi I. A., Fries M., Gainsforth Z., Gallien J.-P., Genge M., Gilles M. K., Gillet P., Gilmour J., Glavin D. P., Gounelle M., Grady M. M., Graham G. A., Grant P. G., Green S. F., Grossemy F., Grossman L., Grossman J. N., Guan Y., Hagiya K., Harvey R., Heck P., Herzog G. F., Hoppe P., Hörz F., Huth J., Hutcheon I. D., Ignatyev K., Ishii H., Ito M., Jacob D., Jacobsen C., Jacobsen S., Jones S., Joswiak D., Jurewicz A., Kearsley A. T., Keller L. P., Khodja H., Kilcoyne A. L. D., Kissel J., Krot A., Langenhorst F., Lanzirotti A., Le L., Leshin L. A., Leitner J., Lemelle L., Leroux H., Liu M.-C., Luening K., Lyon I., MacPherson G., Marcus M. A., Marhas K., Marty B., Matrajt G., McKeegan K., Meibom A., Mennella V., Messenger K., Messenger S., Mikouchi T., Mostefaoui S., Nakamura T., Nakano T., Newville M., Nittler L. R., Ohnishi I., Ohsumi K., Okudaira K., Papanastassiou D. A., Palma R., Palumbo M. E., Pepin R. O., Perkins D., Perronnet M., Pianetta P., Rao W., Rietmeijer F. J. M., Robert F., Rost D., Rotundi A., Ryan R., Sandford S. A., Schwandt C. S., See T. H., Schlutter D., Sheffield-Parker J., Simionovici A., Simon S., Sitnitsky I., Snead C. J., Spencer M. K., Stadermann F. J., Steele A., Stephan T., Stroud R., Susini J., Sutton S. R., Suzuki Y., Taheri M., Taylor S., Teslich N., Tomeoka K., Tomioka N., Toppani A., Trigo-Rodríguez J. M., Troadec D., Tsuchiyama A., Tuzzolino A. J., Tyliszczak T., Uesugi K., Velbel M., Vellenga J., Vicenzi E., Vincze L., Warren J., Weber I., Weisberg M., Westphal A. J., Wirick S., Wooden D., Wopenka B., Wozniakiewicz P., Wright I., Yabuta H., Yano H., Young E. D., Zare R. N., Zega T., Ziegler K., Zimmerman L., Zinner E., and Zolensky M. 2006. Comet 81P/Wild 2 under a microscope. *Science* 314:1711–1716.

Busemann H., Young A., Alexander C. M. O'D., Hoppe P., Muckhopadhyay S., and Nitter L. R. 2006. Interstellar chemistry recorded in organic matter from primitive meteorites. *Science* 312:726–730.

Cody G. D. 2000. Probing chemistry within the membrane structure of wood with soft X-ray spectral microscopy. In *X-ray microscopy,* edited by Meyer-Ilse W., Warwick T., and Attwood D. Melville, New York: American Institute of Physics. 767 p.

Cody G. D. and Alexander C. M. O'D. 2005. NMR studies of chemical structural variation of insoluble organic matter from different carbonaceous chondrite groups. *Geochimica et Cosmochimica Acta* 69:3711–3721.

Cody G. D., Botto R. E., Ade H., and Wirick S. 1996. The application of soft X-ray microscopy to the in situ analysis of sporinite in coal. *International Journal of Coal Geology* 32:69–86.

Feser M., Wirick S., Flynn G. J., and Keller L. P. 2003. Combined carbon, nitrogen, and oxygen XANES spectroscopy on hydrated and anhydrous interplanetary dust particles (abstract #1875). 34th Lunar and Planetary Science Conference. CD-ROM.

Flynn G. J., Bleuet P., Borg J., Bradley J. P., Brenker F. E.,

Brennan S., Bridges J., Brownlee D. E., Bullock E. S., Burghammer M., Clark B. C., Dai Z. R., Daghlian C. P., Djouadi Z., Fakra S., Ferroir T., Floss C., Franchi I. A., Gainsforth Z., Gallien J.-P., Gillet Ph., Grant P. G., Graham G. A., Green S. F., Grossemy F., Heck P. R., Herzog G. F., Hoppe P., Hörz F., Huth J., Ignatyev K., Ishii H. A., Janssens K., Joswiak D., Kearsley A. T., Khodja H., Lanzirotti A., Leitner J., Lemelle L., Leroux H., Luening K., MacPherson G. J., Marhas K. K., Marcus M. A., Matrajt G., Nakamura T., Nakamura-Messenger K., Nakano T., Newville M., Papanastassiou D. A., Pianetta P., Rao W., Riekel C., Rietmeijer F. J. M., Rost D., Schwandt C. S., See T. H., Sheffield-Parker J., Simionovici A., Sitnitsky I., Snead C. J., Stadermann F. J., Stephan T., Stroud R. M., Susini J., Suzuki Y., Sutton S. R., Taylor S., Teslich N., Troadec D., Tsou P., Tsuchiyama A., Uesugi K., Vekemans B., Vicenzi E. P., Vincze L., Westphal A. J., Wozniakiewicz P., Zinner E., and Zolensky M. E. 2006. Elemental compositions of comet 81P/Wild 2 samples collected by Stardust. *Science* 314: 1731–1735.

Flynn G. J., Kellor L. P., Feser M., Wirick S., and Jacobsen C. 2003. The origin of organic matter in the solar system: Evidence from the interplanetary dust particles. *Geochimica et Cosmochimica Acta* 67:4791–4806.

Henke B. L., Gullickson E. M., and Davis J. C. 1993. X-ray interactions: Photoabsorption, scattering, transmission, and reflection at E = 50–30,000 eV, Z = 1-92. *Atomic Data and Nuclear Data Tables* 54:181–342.

Hitchcock A. P. and Mancini D. C. 1994. Bibliography and databases of inner shell excitation spectra of gas phase atoms and molecules. *Journal of Electron Spectroscopy* 67:1–123.

Hörz F., Bastien R., Borg J., Bradley J. P., Bridges J. C., Brownlee D. E., Burchell M. J., Chi M., Cintala M. J., Dai Z. R., Djouadi Z., Dominguez D., Economou T. E., Fairey S. A. J., Floss C., Franchi I. A., Graham G. A., Green S. F., Heck P., Hoppe P., Huth J., Ishii H., Kearsley A. T., Kissel J., Leitner J., Leroux H., Marhas K., Messenger K., Schwandt C. S., See T. H., Snead C., Stadermann F. J., Stephan I. T., Stroud R., Teslich N., Trigo-Rodríguez J. M., Tuzzolino A. J., Troadec D., Tsou P., Warren J., Westphal A., Wozniakiewicz P., Wright I., and Zinner E. 2006. Impact features on Stardust: Implications for comet 81P/Wild 2 dust. *Science* 314:1716–1719.

Jacobsen C., Flynn G. J., Wirick S., and Zimba C. 2000 Soft X-ray spectroscopy from image sequences with sub-100 nm spatial resolution. *Journal of Microscopy* 197:173–184.

Jacobsen C., Williams S., Anderson E., Browne M. T., Buckley C. J., Kern D., Kirz J., Rivers M., and Zhang X. 1991. Diffraction limited imaging in a scanning X-ray microscope. *Optics Communication* 86:351–359.

Keller L. P., Messenger S., Flynn G. F., Clemett S., Wirick S., and Jacobsen C. 2004. The nature of molecular cloud material in interplanetary dust. *Geochimica et Cosmochimica Acta* 68:2577–2589.

Kilcoyne A. L. D., Tyliszczak T., Steele W. F., Fakra S., Hitchcock P., Franck K., Anderson E., Harteneck B., Rightor E. G., Mitchell G. E., Hitchcock A. P., Yang L., Warwick T., and Ade H. 2003. Interferometer controlled scanning transmission microscopes at the advanced light source. *Journal of Synchrotron Radiation* 10:125–136.

McKeegan K. D., Aléon J., Bradley J., Brownlee D., Busemann H., Butterworth A., Chaussidon M., Fallon S., Floss C., Gilmour J., Gounelle M., Graham G., Guan Y., Heck P. R., Hoppe P., Hutcheon I. D., Huth J., Ishii H., Ito M., Jacobsen S. B., Kearsley A., Leshin L. A., Liu M.-C., Lyon I., Marhas K., Marty B., Matrajt G., Meibom A., Messenger S., Mostefaoui S., Mukhopadhyay S., Nakamura-Messenger K., Nittler L., Palma R., Pepin R. O., Papanastassiou D. A., Robert F., Schlutter D., Snead C. J., Stadermann F. J., Stroud R., Tsou P., Westphal A., Young E. D., Ziegler K., Zimmermann L., and Zinner E. 2006. Isotopic compositions of cometary matter returned by Stardust. *Science* 314:1724–1727.

Myneni S. C. B. 2002. Applications of synchrotron radiation in low temperature. *Geochemistry and Environmental Sciences* 49: 485–579.

Rietmeijer F. J. M. 1998. Interplanetary dust particles. In *Planetary materials*, edited by Papike J. J. Reviews in Mineralogy, vol. 36. 95 p.

Sandford S., Aléon J., Alexander C. M. O'D., Araki T., Bajt S., Baratta G. A., Borg J., Bradley J. P., Brownlee D. E., Brucato J. R., Burchell M. J., Busemann H., Butterworth A., Clemett S. J., Cody G., Colangeli L., Cooper G., D'Hendecourt L., Djouadi Z., Dworkin J. P., Ferrini G., Fleckenstein H., Flynn G. J., Franchi I. A., Fries M., Gilles M. K., Glavin D. P., Gounelle M., Grossemy F., Jacobsen C., Keller L. P., Kilcoyne A. L. D., Leitner J., Matrajt G., Meibom A., Mennella V., Mostefaoui S., Nittler L. R., Palumbo M. E., Papanastassiou D. A., Robert F., Rotundi A., Snead C. J., Spencer M. K., Stadermann F. J., Steele A., Stephan T., Tsou P., Tyliszczak T., Westphal A. J., Wirick S., Wopenka B., Yabuta H., Zare R. N., and Zolensky M. E. 2006. Organics captured from comet 81P/Wild 2 by the stardust Spacecraft. *Science* 314:1720–1724.

Stohr J. 1991. *NEXAFS spectroscopy.* New York: Springer. 291 p.

Thompson A. C. and Vaughan D., eds. 2001. *X-ray data booklet.* Berkeley: University of California. 457 p.

Urquhart S. G. and Ade H. 2002. Trends in the Carbonyl core (C1s, O1s) to π^* transition in the near-edge X-ray absorption fine structure spectra of organic molecules. *Journal of Physical Chemistry B* 106:8531–8538.

Van Krevelan D. W. 1993. *Coal*. New York: Elsevier. 1002 p.

Westphal A. J., Snead C., Butterworth A., Graham G. A., Bradley J. P., Bajt S., Grant P. G., Bench G., Brennan S., and Pianetta P. 2004. Aerogel keystones: Extraction of complete hypervelocity impact events from aerogel collectors. *Meteoritics & Planetary Science* 39:1375–1386.

Zolensky M. E., Zega T. J., Yano H., Wirick S., Westphal A. J., Weisberg M. K., Weber I., Warren J. L., Velbel M. A., Tsuchiyama A., Tsou P., Toppani A., Tomioka N., Tomeoka K., Teslich N., Taheri M., Susini J., Stroud R., Stephan T., Stadermann F. J., Snead C. J., Simon S. B., Simionovici A., See T. H., Robert F., Rietmeijer F. J. M., Rao W., Perronnet M. C., Papanastassiou D. A., Okudaira K., Ohsumi K., Ohnishi I., Nakamura-Messenger K., Nakamura T., Mostefaoui S., Mikouchi T., Meibom A., Matrajt G., Marcus M. A., Leroux H., Lemelle L., Le L., Lanzirotti A., Langenhorst F., Krot A. N., Keller L. P., Kearsley A. T., Joswiak D., Jacob D., Ishii H., Harvey R., Hagiya K., Grossman L., Grossman J. N., Graham G. A., Gounelle M., Gillet Ph., Genge M. J., Flynn G., Ferroir T., Fallon S., Ebel D. S., Dai Z. R., Cordier P., Clark B., Chi M., Butterworth A. L., Brownlee D. E., Bridges J. C., Brennan S., Brearley A., Bradley J. P., Bleuet P., Bland P. A., and Bastien R. 2006. Mineralogy and petrology of comet 81P/Wild 2 nucleus samples. *Science* 314:1735–1739.